Available online at www.sciencedirect.com
ScienceDirect
Geochimica et Cosmochimica Acta 73 (2009) 6952–6964
Geochimica et Cosmochimica Acta
www.elsevier.com/locate/gca

A method to estimate the composition of the bulk silicate Earth in the presence of a hidden geochemical reservoir

Jun Korenaga *

Department of Geology and Geophysics, Yale University, P.O. Box 208109, New Haven, CT 06520-8109, USA

Received 22 December 2008; accepted in revised form 14 August 2009; available online 23 August 2009

Abstract

The possibility of a hidden geochemical reservoir in the deep mantle has long been debated in geophysics and geochemistry, because of its bearings on the structure of the core–mantle boundary region, the origin of hotspots, the style of mantle convection, the history of the geomagnetic field, and the thermal evolution of Earth. The presence of such hidden reservoir, however, may invalidate existing models for the composition of the bulk silicate Earth because these models invariably assume that major chemical differentiation in the mantle follows the compositional trend exhibited by upper-mantle rocks. This article presents a new method to estimate the composition of the bulk silicate Earth by explicitly taking into account the possibility of a hidden reservoir. This geochemical inference is formulated as a nonlinear inverse problem, for which an efficient Markov chain Monte Carlo algorithm is developed. Inversion results indicate that the formation of a hidden reservoir, if any, took place at low pressures probably within the first 10 Myr of the history of the solar system and was subsequently lost from the Earth by impact erosion. The global mass balance of the bulk silicate Earth is revisited with the inversion results, and the depletion of highly incompatible elements in the present-day Earth is suggested to be moderate.

1. INTRODUCTION

Heat production within Earth's mantle by four radiogenic isotopes, ^{238}U, ^{235}U, and ^{232}Th, and ^{40}K, is essential to define the thermal budget of Earth, which has controlled the long-term evolution of this planet as a whole (Schubert et al., 2001; Korenaga, 2008). A balance between internal heat production and surface heat flux, for example, determines the rate of secular cooling, which in turn regulates the activity of geodynamo, thus the strength of the magnetic field over Earth's history (Stevenson et al., 1983). The abundance of these heat-producing isotopes has been constrained by composition models for the bulk silicate Earth (BSE), which represents the solid Earth excluding the core. The use of this geochemical constraint, however, requires us to assume how BSE differentiated into various present-day silicate reservoirs such as continental crust and depleted mantle. This issue was raised recently by Lyubetskaya and Korenaga (2007a,b), but its significance has not been fully explored yet. It is not a very obvious problem either, because it involves both how BSE composition models have been estimated and how mantle convection models have evolved in the last few decades. Put simply, if geophysical considerations are taken into account, the standard way of estimating the BSE composition may not be compatible with the existence of a hidden geochemical reservoir, which has been popular in the literature.

To understand this issue, let us first review briefly how the BSE composition has been estimated (see Lyubetskaya and Korenaga (2007a), for a more extensive version). A central procedure, which is common to the majority of existing models (McDonough and Sun, 1995; Palme and O'Neill, 2003; Lyubetskaya and Korenaga, 2007a), is to impose cosmochemical constraints (the ratios of refractory lithophile elements (RLEs) in carbonaceous chondrites) on compositional trends exhibited by upper-mantle rocks such as mantle xenoliths and massif peridotites (Fig. 1a). RLEs, which include rare earth elements as well as U and

* Tel.: +1 203 432 7381; fax: +1 203 432 3134.
E-mail address: jun.korenaga@yale.edu

0016-7037/$ - see front matter © 2009 Elsevier Ltd. All rights reserved.
doi:10.1016/j.gca.2009.08.020

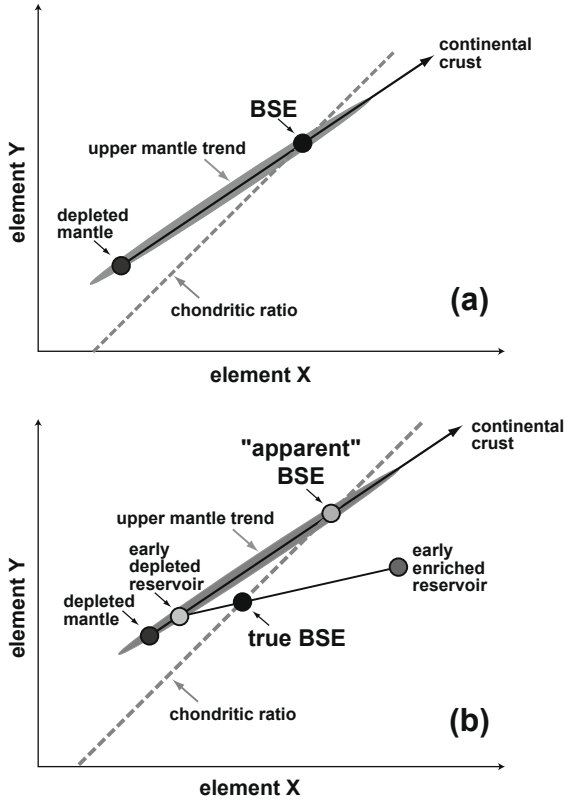

Fig. 1. Schematic co-variation diagrams to illustrate the difficulty of estimating the BSE composition if a hidden reservoir such as EER exists. (a) How BSE has been estimated in previous studies. Elements X and Y here are both refractory lithophile elements, so we expect their BSE compositions to have a chondritic ratio. (b) If BSE differentiated into EER and EDR in the early Earth, BSE does not have to be found along the composition trend exhibited by upper-mantle rocks (unless the chemical differentiation that produced EER and EDR happens to have the trend of upper-mantle rocks—this cannot be assumed *a priori* because there is no terrestrial sample representing EER). It is still possible to impose a chondritic ratio on the trend to find the "apparent" BSE composition, though it could be very different from the true BSE composition.

Th, have very high condensation temperature and also do not enter the core because they are favored by silicate phases. The RLE ratios are fairly constant among different types of carbonaceous chondrites, and it is reasonable to expect that BSE shares similar ratios given plausible planetary accretion processes. It is customary to use the RLE composition of CI chondrites in this procedure. The RLE ratios of BSE do not have to be *exactly* the same as those of CI chondrites, and the method of Lyubetskaya and Korenaga (2007a) is the first to explicitly take into account such uncertainty. At any rate, this procedure identifies the location of BSE within the upper mantle trend in terms of (a few selected) RLEs (Fig. 1a), which may then be used to estimate the BSE concentration of other RLEs as well as nonRLEs. BSE is commonly found to have ~2–3 times higher concentration of RLEs than CI chondrites. This degree of enrichment in BSE is expected because of the loss of volatile elements during planetary accretion and because of the segregation of the core. The BSE contents of U and Th have been estimated assuming the same enrichment factor for all RLEs (i.e., RLEs did not fractionate to each other when BSE was created); owing to various difficulties, they are not estimated directly from their concentrations in upper-mantle rocks.

A potential problem of the above approach is that only upper-mantle rocks are used, because there is no direct sample from the transition zone or the lower mantle. If Earth's mantle is well mixed by convection (i.e., whole mantle convection), sampling only from the upper mantle is not a concern, but if not, we may have a difficult situation depending on what kind of layered convection we assume. For a traditional layered mantle model (e.g., Jacobsen and Wasserburg, 1979; DePaolo, 1980; Allegre, 2002), for example, the upper mantle is depleted as inferred from mid-ocean ridge basalts (MORB) and is thought to be complementary to the continental crust, whereas the lower mantle is assumed to be primitive, i.e., having the undifferentiated BSE composition. Although geochemical constraints on the mass fraction of the depleted mantle have been known to be rather weak (Allegre et al., 1983; Zindler and Hart, 1986), the notion of relatively more primitive lower mantle has long been popular. Note that the depleted mantle is depleted in incompatible elements but has a major element composition very similar to BSE, because the extraction of continental crust has little impact on the major element budget. For this type of layered model, therefore, the use of upper-mantle rocks does not seem to pose a problem, as far as geochemistry is concerned.

A fundamental difficulty arises, however, when we consider the physical plausibility of such layered mantle. How can the mantle remain dynamically layered if the upper and lower mantle have virtually the same major element composition? A popular argument used to be that mass transport between them may be hampered by an endothermic phase change expected at the base of the transition zone (e.g., Christensen and Yuen, 1984), but for this mechanism to be effective, the Clapeyron slope of the phase change must be much more negative (<-6 MPa K^{-1}) than mineral physics supports (-1.3 MPa K^{-1}, Katsura et al., 2003; Fei et al., 2004). Moreover, seismic tomography suggests that at least some of subducted slabs do penetrate into the lower mantle (e.g., van der Hilst et al., 1997; Fukao et al., 2001), so the endothermic phase change does not seem to serve as a barrier for material transport. In recent layered models, therefore, the upper and lower layers do not necessarily coincide with the upper and lower mantle, and the boundary between these two layers is often hypothesized to locate somewhere in the lower mantle (e.g., Kellogg et al., 1999). Other potential layering mechanisms such as higher viscosity in the deep mantle and depth-dependent thermal properties have also been explored (e.g., van Keken and Ballentine, 1998; Hunt and Kellogg, 2001; Naliboff and Kellogg, 2007), but it is always found to be difficult to maintain mantle layering without invoking *intrinsic* density stratification, i.e., stratification in major element composition. In this case, the major element composition of the lower layer must be substantially different from that of the upper layer (e.g.,

by being enriched in iron), which is at odds with the conventional notion of the primitive lower mantle. The lower layer cannot be primitive, and we need to consider how BSE differentiated into the upper and lower layers. If this differentiation took place at relatively low pressures, it may still be valid to seek the location of BSE within the upper mantle trend. This is an important assumption, however, which is hereinafter referred to as the common trend assumption.

The recent discovery of ^{142}Nd difference between chondrites and terrestrial rocks implies that a deep reservoir (i.e., the lower layer) must have been created by global-scale differentiation in the very early Earth (within the first 30 Myr or so) and that it has been isolated almost completely (Boyet and Carlson, 2005). In this case, it is not easy to justify the common trend assumption because the hidden reservoir could have been created by ultra-high-pressure differentiation in the early Earth (Labrosse et al., 2007), which does not have to follow the composition trend of upper-mantle rocks (Corgne et al., 2005). In case of layered mantle convection (or in the presence of a hidden geochemical reservoir), therefore, the conventional way to estimate the BSE composition could provide us an erroneous answer (Fig. 1b). Imposing a chondritic ratio on the upper mantle trend would give us only the "apparent" BSE composition, which does not have to coincide with the true BSE composition. We may have been incorrectly estimating the enrichment factor for RLEs and thus the heat production of BSE; this is a critical issue for both geochemistry (global mass balance) and geophysics (thermal budget).

If we cannot justify the common trend assumption, the BSE composition itself becomes undefined, because the assumption is implicit in existing BSE models. To better appreciate this, consider the following mass balance argument. If we estimate the composition of the present-day mantle (PDM) based on mid-ocean ridge basalts (MORB) (Jochum et al., 1983; Salters and Stracke, 2004) or abyssal peridotites (Workman and Hart, 2005), PDM is usually shown to be so depleted in incompatible elements that adding continental crust (CC) to PDM does not recover BSE, pointing to the presence of a deeply-hidden enriched reservoir. Then, the composition of the hidden reservoir, C_{hidden}, is usually estimated based on the following relation (or something equivalent) (e.g., Boyet and Carlson, 2006; Labrosse et al., 2007):

$$C_{\mathrm{BSE}} = f_{\mathrm{CC}} C_{\mathrm{CC}} + f_{\mathrm{PDM}} C_{\mathrm{PDM}} + f_{\mathrm{hidden}} C_{\mathrm{hidden}}, \quad (1)$$

where f_i denotes the mass fraction of each reservoir, and

$$f_{\mathrm{CC}} + f_{\mathrm{PDM}} + f_{\mathrm{hidden}} = 1. \quad (2)$$

This exercise is commonly seen in the literature, but it is valid only when we can justify the common trend assumption. Without this assumption, the composition of the true BSE (C_{BSE}) is undefined, and we need to consider a more general situation such as shown in Fig. 1b. But in this case, using existing BSE models in Eq. (1) would be equivalent to using the apparent BSE composition in Fig. 1b; the hidden reservoir is always found (incorrectly) along the upper mantle trend by this mass balance.

We thus seem to be in a quandary. The possibility of a hidden geochemical reservoir in the deep mantle is intriguing because of its bearings on the structure of the core–mantle boundary region, the origin of hotspots, the style of mantle convection, the history of the geomagnetic field, and the thermal evolution of Earth. If we hypothesize such reservoir, however, the (true) BSE composition can be different from the conventional estimate, and the composition of the hidden reservoir becomes undefined. This is why exploring the consequence of layered mantle convection is regarded as an arbitrary exercise (Korenaga, 2008). The difference between the 'apparent' and 'true' BSE compositions (Fig. 1b) may be small, but such difference needs to be quantified. The purpose of this paper is to resolve this situation by devising a new self-consistent method of estimating the BSE composition, which explicitly takes into account the possibility of a hidden reservoir. In place of the common trend assumption, the proposition by Boyet and Carlson (2005) that Earth experienced early global differentiation is adopted. Note that the formation of a hidden reservoir by early Earth differentiation is not the unique interpretation of the ^{142}Nd data (e.g., Ranen and Jacobsen, 2006; Bourdon et al., 2008; Caro et al., 2008; Warren, 2008). Our strategy is to adopt the early Earth differentiation as a working hypothesis and see where it leads us. As discussed later, our results seem to provide an intriguing justification for the common trend assumption, and its implications for the Earth's chemical budget will be explored.

Also, in addition to the ^{142}Nd argument, there are several other mass balance arguments for a hidden geochemical reservoir such as the missing Ar paradox (Allegre et al., 1996; Lassiter, 2004), the missing heat source paradox (Kellogg et al., 1999; Turcotte et al., 2001), the helium and heat flux imbalance (O'Nions and Oxburgh, 1983), and the Pb paradoxes (Hofmann, 2003). Except for the last one, which may simply reflect protracted core formation (Galer and Goldstein, 1996; Halliday, 2000) or the incomplete characterization of the Pb budget in silicate reservoirs (Rudnick and Goldstein, 1990; Malaviarachchi et al., 2008), these arguments have been shown to be sensitive to the choice of a BSE composition model (Lyubetskaya and Korenaga, 2007b). In the discussion section, therefore, we will revisit these arguments as well.

2. METHOD

2.1. Basic equations

Similar to the differentiation scenario advocated by Boyet and Carlson (2005), it is assumed that BSE first differentiated into an early enriched reservoir (EER) and an early depleted reservoir (EDR), and that EDR then differentiated into the continental crust (CC) and the present-day accessible mantle (PDAM) over Earth's history (Fig. 2). It follows that $m_{\mathrm{BSE}} = m_{\mathrm{EER}} + m_{\mathrm{EDR}} = m_{\mathrm{EER}} + m_{\mathrm{PDAM}} + m_{\mathrm{CC}}$, where m_x denotes the mass of a reservoir x, or in terms of mass fraction,

$$f_{\mathrm{EER}} + f_{\mathrm{EDR}} = 1, \quad (3)$$

and

$$f_{\mathrm{PDAM}} + f_{\mathrm{CC}} = f_{\mathrm{EDR}}, \quad (4)$$

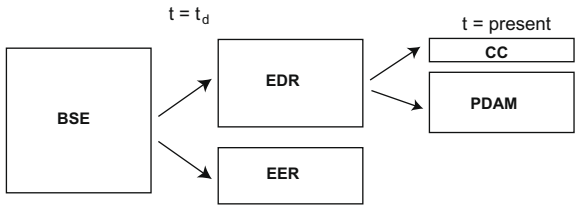

Fig. 2. Two-stage mantle differentiation scenario assumed in this study. The bulk silicate Earth first differentiates into an early depleted reservoir (EDR) and an early enriched reservoir (EER) at $t = t_d$, and EDR then differentiates into the continental crust (CC) and the present-day accessible mantle (PDAM) throughout the rest of Earth's history.

where f_{CC} is 0.0058, with m_{BSE} of 4.0×10^{24} kg and m_{CC} of 2.3×10^{22} kg.

Here PDAM is defined as a residual after extracting CC from EDR, and it may be called simply as the depleted mantle (DM) because it is depleted by the extraction of continental crust. However, it appears that the term DM is often considered synonymous with the depleted MORB source mantle (DMM), and if we use DM instead of PDAM in the above, some might be mistaken that we are ignoring a more enriched source mantle for ocean island basalts (OIB), which may be referred collectively as the enriched mantle (EM). A few different kinds of OIB source mantle have been proposed (e.g., Zindler and Hart, 1986), and my use of EM here is meant to encompass all of them. If there is no 'hidden' mantle reservoir, PDAM is equivalent to PDM. The adjective 'accessible' in PDAM is to signify its contrastive nature to the putative 'hidden' reservoir. On average, PDAM is depleted in elements enriched in continental crust, but there can be spatial variation in the degree of depletion because of a complex history of mantle melting and mixing (e.g., Anderson et al., 1992; Korenaga, 2004, 2005; Ito and Mahoney, 2005). Different source mantles for MORB and OIB may represent such spatial variation, and PDAM is a volumetric average of all kinds of source mantle responsible for terrestrial magmatism, including DMM, EM, and other more exotic mantle components.

There are two kinds of differentiation (BSE → EER + EDR, and EDR → CC + PDAM), and each differentiation should satisfy one elemental mass balance of Nd and three isotopic mass balances of ($^{147}Sm/^{144}Nd$), ($^{143}Nd/^{144}Nd$), and ($^{142}Nd/^{144}Nd$). As ($^{147}Sm/^{144}Nd$) may be converted to the elemental ratio Sm/Nd by multiplying 1.6552, the first isotopic mass balance is equivalent to the Sm mass balance. For EDR = CC + PDAM, there are thus four mass-balance relations:

$$f_{EDR} C_{Nd}^{EDR} = f_{CC} C_{Nd}^{CC} + f_{PDAM} C_{Nd}^{PDAM}, \tag{5}$$

$$f_{EDR} C_{Nd}^{EDR} \left(\frac{^{147}Sm}{^{144}Nd}\right)^{EDR} = f_{CC} C_{Nd}^{CC} \left(\frac{^{147}Sm}{^{144}Nd}\right)^{CC} + f_{PDAM} C_{Nd}^{PDAM} \left(\frac{^{147}Sm}{^{144}Nd}\right)^{PDAM}, \tag{6}$$

$$f_{EDR} C_{Nd}^{EDR} \left(\frac{^{143}Nd}{^{144}Nd}\right)^{EDR} = f_{CC} C_{Nd}^{CC} \left(\frac{^{143}Nd}{^{144}Nd}\right)^{CC} + f_{PDAM} C_{Nd}^{PDAM} \left(\frac{^{143}Nd}{^{144}Nd}\right)^{PDAM}, \tag{7}$$

and

$$f_{EDR} C_{Nd}^{EDR} \left(\frac{^{142}Nd}{^{144}Nd}\right)^{EDR} = f_{CC} C_{Nd}^{CC} \left(\frac{^{142}Nd}{^{144}Nd}\right)^{CC} + f_{PDAM} C_{Nd}^{PDAM} \left(\frac{^{142}Nd}{^{144}Nd}\right)^{PDAM}, \tag{8}$$

where C_{Nd}^{x} denotes the Nd concentration in a reservoir x. The Nd and Sm isotopes of EDR are also constrained by the following decay equations (e.g., Caro et al., 2003):

$$\left(\frac{^{143}Nd}{^{144}Nd}\right)^{EDR} = \left(\frac{^{143}Nd}{^{144}Nd}\right)^{BSE} + \left(\frac{^{147}Sm}{^{144}Nd}\right)^{BSE} \left[1 - \exp(\lambda_{147}(t_p - t_d))\right] + \left(\frac{^{147}Sm}{^{144}Nd}\right)^{BSE} \left[\exp(\lambda_{147}(t_p - t_d)) - 1\right], \tag{9}$$

and

$$\left(\frac{^{142}Nd}{^{144}Nd}\right)^{EDR} = \left(\frac{^{142}Nd}{^{144}Nd}\right)^{BSE} - \frac{\left(\frac{^{146}Sm}{^{144}Sm}\right)_i^{BSE}}{\left(\frac{^{147}Sm}{^{144}Nd}\right)^{BSE}} \left\{ \left(\frac{^{147}Sm}{^{144}Nd}\right)^{BSE} \exp(-\lambda_{146} t_d) + \left(\frac{^{147}Sm}{^{144}Nd}\right)^{EDR} \left[\exp(-\lambda_{146} t_p) - \exp(-\lambda_{146} t_d)\right] \right\}, \tag{10}$$

where λ_{147} is 6.54×10^{-12} year^{-1}, λ_{146} is 6.74×10^{-9} year^{-1}, t_p is the age of the solar system (4.568 Gyr, Burkhardt et al., 2008), and t_d is the time of global differentiation measured from the beginning of the solar system. All isotopic ratios are present-day values, unless marked by a subscript i, which denotes an initial value. Here time t is measured forward, so our t_d, t_p, and $t_p - t_d$ correspond to, respectively, $t_0 - t_d$, $t_0 - t_p$, and t_d in the formulation by Caro et al. (2003), in which t is age measured from the present. ($^{147}Sm/^{144}Sm)^{BSE}$ in Eq. (10) may be calculated as ($^{147}Sm/^{144}Nd)^{BSE}$/($^{144}Sm/^{144}Nd)^{BSE}$, for which ($^{144}Sm/^{144}Nd)^{BSE}$ of 0.04033 (Jacobsen and Wasserburg, 1984) is used. Deriving similar evolutionary constraints for CC and PDAM is not attempted because their isotopic evolution is likely to be much more complex due to time-varying differentiation and recycling. The mass-fraction relation of (4) and the above six Eqs. (5)–(10), taken together, have the following unknown variables: f_{PDAM}, f_{EDR}, t_d, C_{Nd}^{EDR}, C_{Sm}^{EDR}, ($^{143}Nd/^{144}Nd)^{EDR}$, and ($^{142}Nd/^{144}Nd)^{EDR}$. Because there are the same number of equations and unknowns, these seven unknowns may be uniquely determined by specifying other variables related to CC, PDAM, and BSE. We further impose the following constraint at the present day:

$$\left(\frac{^{143}Nd}{^{144}Nd}\right)^{EDR} < \max\left(\frac{^{143}Nd}{^{144}Nd}\right)^{EDR}, \quad (11)$$

to be consistent with the Nd isotopic evolution of PDAM as inferred from juvenile granites and Phanerozoic ophiolites (Bennett, 2003). The right-hand side of this inequality corresponds to the largest $\varepsilon^{143}Nd^{PDAM}$ value suggested for the early Archean (i.e., ~4). The BSE isotopic ratios are assumed to be identical to the chondrite values, with their *a priori* ranges determined by statistical uncertainties reported in the literature (see Table 1). One notable exception is that the *a priori* range of $\varepsilon^{142}Nd^{BSE}$ is based on 1σ (0.07), not 2σ (0.14) reported by Boyet and Carlson (2005). If we use 2σ instead, $\varepsilon^{142}Nd^{BSE}$ would almost overlap with the PDAM and CC values of $\varepsilon^{142}Nd^{BSE}$, nullifying the need for a hidden reservoir. In the same spirit, we use the range of $\varepsilon^{142}Nd^{PDAM}$ reported by Caro et al. (2006), which is slightly tighter than that by Boyet and Carlson (2005). The $\varepsilon^{142}Nd$ of OIB has not been measured extensively yet, and we are assuming here that a hidden reservoir does not contribute to the OIB source mantle. This is consistent with our definition of PDAM.

Similarly, for BSE = EER + EDR, there are also one mass-fraction equation (3), four mass-balance equations as

$$C_{Nd}^{BSE} = f_{EER}C_{Nd}^{EER} + f_{EDR}C_{Nd}^{EDR}, \quad (12)$$

$$C_{Nd}^{BSE}\left(\frac{^{147}Sm}{^{144}Nd}\right)^{BSE} = f_{EER}C_{Nd}^{EER}\left(\frac{^{147}Sm}{^{144}Nd}\right)^{EER} + f_{EDR}C_{Nd}^{EDR}\left(\frac{^{147}Sm}{^{144}Nd}\right)^{EDR}, \quad (13)$$

$$C_{Nd}^{BSE}\left(\frac{^{143}Nd}{^{144}Nd}\right)^{BSE} = f_{EER}C_{Nd}^{EER}\left(\frac{^{143}Nd}{^{144}Nd}\right)^{EER} + f_{EDR}C_{Nd}^{EDR}\left(\frac{^{143}Nd}{^{144}Nd}\right)^{EDR}, \quad (14)$$

Table 1
Variables used in MCMC inversion and their probability distributions.

Variable	*A priori* distribution[a]	*A posteriori* distribution[b]
f_{EER}	0–0.8	(0.03, 0.09, 0.23)
t_d (Myr)	0–100	(3.9, 9.0, 17.0)
$\gamma^{147}Sm^{BSE}$[c]	—[d]	(−0.9, −0.6, −0.4)
$(^{146}Sm/^{144}Sm)_i^{BSE}$	0.006–0.009[1,2]	(0.0081, 0.0085, 0.0088)
$\varepsilon^{143}Nd^{PDAM}$[e]	0–15[3]	(5.5, 6.0, 6.6)
$\varepsilon^{143}Nd^{CC}$[e]	−20 to −10 [4]	(−16.6, −14.5, −12.5)
$\varepsilon^{143}Nd^{BSE}$[e]	−1 to 1	(−0.90, −0.76, −0.52)
$\varepsilon^{143}Nd^{EER}$[e]	—[g]	(−30.5, −14.4, −6.8)
$\varepsilon^{143}Nd^{EDR}$[e]	<4[11]	(3.4, 3.7, 3.9)
$\varepsilon^{142}Nd^{PDAM}$[f]	−0.05 to 0.04[5]	(−0.047, −0.044, −0.038)
$\varepsilon^{142}Nd^{CC}$[f]	−0.07 to 0.07[6]	(−0.054, −0.032, 0.001)
$\varepsilon^{142}Nd^{BSE}$[f]	−0.27 to −0.13[6]	(−0.15, −0.14, −0.13)
$\varepsilon^{142}Nd^{EER}$[f]	—[g]	(−0.85, −0.47, −0.28)
$\varepsilon^{142}Nd^{EDR}$[f]	—[g]	(−0.046, −0.041, −0.035)
C_{Nd}^{PDAM} (ppm)	0.58–1.45[7,8,9,12]	(0.81, 0.88, 0.95)
C_{Nd}^{CC} (ppm)	14–26[10]	(14.8, 16.4, 18.9)
C_{Nd}^{BSE} (ppm)	0.23–2.07[h]	(1.1, 1.2, 1.3)
C_{Nd}^{EER} (ppm)	—[g]	$10^{(0.25,\ 0.44,\ 0.75)}$
C_{Nd}^{EDR} (ppm)	—[g]	(0.92, 0.99, 1.06)
C_{Sm}^{PDAM} (ppm)	0.24–0.47[7,8,9,12]	(0.28, 0.30, 0.33)
C_{Sm}^{CC} (ppm)	2.7–5.1[10]	(3.9, 4.5, 4.8)
C_{Sm}^{BSE} (ppm)	0.08 – 0.68[h]	(0.34, 0.37, 0.42)
C_{Sm}^{EER} (ppm)	—[g]	$10^{(-0.33,\ -0.15,\ 0.14)}$
C_{Sm}^{EDR} (ppm)	—[g]	(0.31, 0.33, 0.36)

References: 1, Lugmair and Galer (1992); 2, Prinzhofer et al. (1992); 3, Hofmann (2003); 4, Goldstein et al. (1984); 5, Caro et al. (2006); 6, Boyet and Carlson (2005); 7, Salters and Stracke (2004); 8, Workman and Hart (2005); 9, Langmuir et al. (2005); 10, Rudnick and Gao (2003); 11, Bennett (2003); 12, Palme and O'Neill (2003).

[a] A value is randomly chosen from a given range (i.e., uniform *a priori* distribution).

[b] Three numbers in parentheses are first quartile, median, and third quartile, respectively. See also Fig. 3.

[c] Defined as $((^{147}Sm/^{144}Nd)^{BSE}/(^{147}Sm/^{144}Nd)^{CHUR} - 1) \times 100$, where $(^{147}Sm/^{144}Nd)^{CHUR}$ is 0.1966 (Jacobsen and Wasserburg, 1980, 1984; Patchett et al., 2004). This variable is proportional to the BSE Sm/Nd ratio. CHUR stands for the chondritic uniform reservoir.

[d] The *a priori* distribution for this variable is specified indirectly based on the following relation: $(^{147}Sm/^{144}Nd)^{BSE} = ((^{143}Nd/^{144}Nd)^{BSE} - (^{143}Nd/^{144}Nd)_i^{BSE}/(\exp(\lambda_{147}t_p) - 1)$. $(^{143}Nd/^{144}Nd)^{BSE}$ and $(^{143}Nd/^{144}Nd)_i^{BSE}$ are, respectively, sampled from within ±0.01% and ±0.005% from their CHUR values (Patchett et al., 2004).

[e] Defined with $(^{143}Nd/^{144}Nd)^{CHUR}$ of 0.512638 (Jacobsen and Wasserburg, 1980, 1984; Patchett et al., 2004).

[f] Defined with $(^{142}Nd/^{144}Nd)^{standard}$ of 1.141848 (Boyet and Carlson, 2005).

[g] These variables are the output parameters of the inversion, so their *a priori* distributions do not need to be specified.

[h] These variables are also output parameters, and these *a priori* ranges are used to reject unrealistic solutions during MCMC iterations. These ranges correspond to a fairly wide range of the RLE enrichment factor (0.5–4.5), with the CI chondrite composition of Nd (0.46 ppm) and Sm (0.15 ppm) (Lodders and Fegley, 1998); given the likely effects of evaporation (during planetary accretion) and core segregation, the enrichment factor should be ~2–3 (McDonough and Sun, 1995; Palme and O'Neill, 2003).

and

$$C_{\mathrm{Nd}}^{\mathrm{BSE}}\left(\frac{^{142}\mathrm{Nd}}{^{144}\mathrm{Nd}}\right)^{\mathrm{BSE}} = f_{\mathrm{EER}}C_{\mathrm{Nd}}^{\mathrm{EER}}\left(\frac{^{142}\mathrm{Nd}}{^{144}\mathrm{Nd}}\right)^{\mathrm{EER}} + f_{\mathrm{EDR}}C_{\mathrm{Nd}}^{\mathrm{EDR}}\left(\frac{^{142}\mathrm{Nd}}{^{144}\mathrm{Nd}}\right)^{\mathrm{EDR}}, \quad (15)$$

and two evolutionary constraints on EER as

$$\left(\frac{^{143}\mathrm{Nd}}{^{144}\mathrm{Nd}}\right)^{\mathrm{EER}} = \left(\frac{^{143}\mathrm{Nd}}{^{144}\mathrm{Nd}}\right)^{\mathrm{BSE}} + \left(\frac{^{147}\mathrm{Sm}}{^{144}\mathrm{Nd}}\right)^{\mathrm{BSE}} \times [1-\exp(\lambda_{147}(t_p-t_d))] + \left(\frac{^{147}\mathrm{Sm}}{^{144}\mathrm{Nd}}\right)^{\mathrm{EER}}[\exp(\lambda_{147}(t_p-t_d))-1], \quad (16)$$

and

$$\left(\frac{^{142}\mathrm{Nd}}{^{144}\mathrm{Nd}}\right)^{\mathrm{EER}} = \left(\frac{^{142}\mathrm{Nd}}{^{144}\mathrm{Nd}}\right)^{\mathrm{BSE}} - \frac{\left(\frac{^{146}\mathrm{Sm}}{^{144}\mathrm{Sm}}\right)_i^{\mathrm{BSE}}}{\left(\frac{^{147}\mathrm{Sm}}{^{144}\mathrm{Nd}}\right)^{\mathrm{BSE}}}\left\{\left(\frac{^{147}\mathrm{Sm}}{^{144}\mathrm{Nd}}\right)^{\mathrm{BSE}}\exp(-\lambda_{146}t_d) + \left(\frac{^{147}\mathrm{Sm}}{^{144}\mathrm{Nd}}\right)^{\mathrm{EER}}[\exp(-\lambda_{146}t_p)-\exp(-\lambda_{146}t_d)]\right\}. \quad (17)$$

The number of unknown variables are seven again: f_{EER}, $C_{\mathrm{Nd}}^{\mathrm{EER}}$, $C_{\mathrm{Sm}}^{\mathrm{EER}}$, $C_{\mathrm{Nd}}^{\mathrm{BSE}}$, $C_{\mathrm{Sm}}^{\mathrm{BSE}}$, $(^{143}\mathrm{Nd}/^{144}\mathrm{Nd})^{\mathrm{EER}}$, and $(^{142}\mathrm{Nd}/^{144}\mathrm{Nd})^{\mathrm{EER}}$, but in the presence of the evolutionary constraints (Eqs. (16) and (17)), Eqs. (14) and (15) are redundant with Eqs. (12) and (13). Thus, the number of independent constraints is actually five, and this is an under-determined system of equations. Because EER must be enriched with respect to EDR, however, the following inequality relations should hold:

$$C_{\mathrm{Nd}}^{\mathrm{EER}} > C_{\mathrm{Nd}}^{\mathrm{EDR}}, \quad (18)$$

and

$$C_{\mathrm{Sm}}^{\mathrm{EER}} > C_{\mathrm{Sm}}^{\mathrm{EDR}}, \quad (19)$$

which help to reduce the degree of nonuniqueness substantially.

Some of the 'known' variables, regarding the elemental and isotopic compositions of CC and PDAM, are characterized by nontrivial uncertainties. In particular, PDAM is not equivalent to DMM as noted earlier, so the *a priori* range of the PDAM composition is chosen to cover from the most depleted estimate (Workman and Hart, 2005) to the most enriched BSE composition (Palme and O'Neill, 2003), within which other estimates (Salters and Stracke, 2004; Langmuir et al., 2005) are contained (Table 1). Also, the mass-balance and evolutionary constraints as a whole constitute a system of nonlinear equations. Delineating the permissible solution space for the above 14 unknowns, therefore, is a nonlinear inverse problem, which may be solved efficiently by a Markov chain Monte Carlo algorithm as explained next.

2.2. Markov chain Monte Carlo algorithm

Markov chain Monte Carlo (MCMC) methods refer to a class of guided random walk algorithms based on Markov chains (Liu, 2001; Robert and Cassela, 2004). These methods have long been used in computational physics to numerically evaluate multi-dimensional integrals (e.g., Metropolis et al., 1953; Frenkel and Smit, 2002). As such integrals are at the heart of Bayesian statistics, MCMC methods are now widely used in statistics, and this means that they are also suited to solve nonlinear inverse problems in a statistically comprehensive manner. Because MCMC methods are generally computationally expensive, however, the number of model parameters to be estimated cannot be very large, so their application to geophysical problems is still in its infancy (e.g., Mosegaard and Tarantola, 1995; Sambridge and Mosegaard, 2002; Korenaga and Karato, 2008). Fortunately, the number of unknown parameters in the present geochemical problem is only 14, so the MCMC approach remains viable.

The basic structure of MCMC methods may be summarized as follows:

1. *Initialization.* If the number of model parameters is N, draw N random numbers to prepare the initial model vector $\mathbf{m}_0$.
2. *Random walk.* Take a random step from $\mathbf{m}_0$ and call the new model $\mathbf{m}'$.
3. *Evaluation.* Draw a random number, r, from the interval [0, 1]. If $r < L(\mathbf{m}')/L(\mathbf{m}_0)$, where $L(\mathbf{m})$ denotes the likelihood of a model $\mathbf{m}$, go to the next step. Otherwise, go back to the previous step.
4. *Model update.* Save the old model $\mathbf{m}_0$ and redefine it with $\mathbf{m}'$. Until the maximum number of iteration is reached, go back to Step 2.

The likelihood function L in the evaluation step is what measures the success of a particular model in explaining given constraints. So when the new model $\mathbf{m}'$ can explain the constraints better than the old one $\mathbf{m}_0$, the ratio $L(\mathbf{m}')/L(\mathbf{m}_0)$ is greater than one, so the new model is always accepted in this case. A key point in MCMC is that, even when the new model is worse than the old, there is a nonzero probability of accepting it. This allows us to avoid being trapped in a local minimum during random walk and explore the model space extensively to eventually find *all* important solutions, in the limit of the *infinite* number of iterations. A difficult part is how to implement the above basic steps for a given inverse problem. The random walk step, for example, can be tricky. If a step size is too big, the new likelihood is usually very small, i.e., $L(\mathbf{m}')/L(\mathbf{m}_0) \ll 1$, and the probability of drawing a random number smaller than this ratio is also very low. So it would take a large number of trial random steps to get to the model update step. If a step size is too small instead, it would require a succession of low-probability model updates to escape from a local minimum. In other words, the step size has to be just right to have efficient MCMC iterations. Also, how to design random walk for a set of multiple parameters is not always obvious, and the efficiency of an MCMC algorithm could be largely influenced by an adopted design.

Here one possible MCMC algorithm is provided for the present inverse problem. The problem of step size mentioned above is resolved by adopting the random-scan Gibbs sampling (e.g., Liu, 2001). A few different designs of random walk were also tested, and the one shown below is the most efficient one among those trials. The following 13 variables are used as 'input' parameters: f_{EER}, t_d, $(^{143}\mathrm{Nd}/^{144}\mathrm{Nd})^{\mathrm{BSE}}$, $(^{143}\mathrm{Nd}/^{144}\mathrm{Nd})_i^{\mathrm{BSE}}$, $(^{146}\mathrm{Sm}/^{144}\mathrm{Sm})_i^{\mathrm{BSE}}$, $C_{\mathrm{Sm}}^{\mathrm{CC}}$, $C_{\mathrm{Nd}}^{\mathrm{CC}}$, $r_{\mathrm{Sm/Nd}}^{\mathrm{PDAM}}$, $C_{\mathrm{Nd}}^{\mathrm{PDAM}}$, $(^{143}\mathrm{Nd}/^{144}\mathrm{Nd})^{\mathrm{PDAM}}$, $(^{142}\mathrm{Nd}/^{144}\mathrm{Nd})^{\mathrm{CC}}$, $(^{142}\mathrm{Nd}/^{144}\mathrm{Nd})^{\mathrm{PDAM}}$, and $r_{\mathrm{Sm/Nd}}^{\mathrm{EER}}$, where $r_{\mathrm{Sm/Nd}}^{\mathrm{PDAM}}$ and $r_{\mathrm{Sm/Nd}}^{\mathrm{EER}}$ are the Sm/Nd ratio for PDAM and EER, respectively, normalized by the BSE ratio. These parameters will be referred to collectively as $\mathbf{m}$.

1. *Initialization.* Draw $N(=13)$ random numbers, r_k, from the interval [0, 1] to set the initial model as

$$m_{0,k} = m_k^L + r_k\left(m_k^U - m_k^L\right),$$

for $k = 1,2,\ldots,N$, where m_k^U and m_k^L are the upper and lower limits, respectively, of a model parameter m_k (see Table 1).

2. *Random scan.* Pick one model parameter randomly from $\{m_k | k = 1,2,\ldots,N\}$ and call it m_r. The random-scan Gibbs sampling requires that we know the conditional likelihood:

$$L(\{m_{0,1},\ldots,m_{0,r-1},m_r,m_{0,r+1},\ldots,m_{0,N}\}).$$

All parameters other than m_r are fixed as in the current model $\mathbf{m}_0$, and the conditional likelihood is a function of m_r only. From the interval $[m_r^L, m_r^U]$, we draw P random numbers and calculate corresponding likelihood values. When P is sufficiently large, we can approximate the conditional likelihood function by the rejection sampling (von Neumann, 1951). Save the highest likelihood as $L_{\max}$.

3. *Gibbs sampling*. Pick one random number from the interval $[m_r^L, m_r^U]$ and call it m_r'. Construct a trial model:

$$\mathbf{m}' = \{m_{0,1},\ldots,m_{0,r-1},m_r',m_{0,r+1},\ldots,m_{0,N}\}$$

and calculate $L(\mathbf{m}')$. Draw one more random number, s, from the interval [0, 1]. If $s < L(\mathbf{m}')/L_{\max}$, go to the next step. Otherwise, start over this step.

4. *Model update.* Save the old model $\mathbf{m}_0$ and redefine it with $\mathbf{m}'$. Until the maximum number of iteration is reached, go back to Step 2.

The likelihood $L(\mathbf{m})$ is calculated as follows:

1. *Parameter conversion.* The input model parameters are converted to the following variables: $(^{147}\mathrm{Sm}/^{144}\mathrm{Nd})^{\mathrm{BSE}}$, $(^{147}\mathrm{Sm}/^{144}\mathrm{Sm})^{\mathrm{BSE}}$, $(\mathrm{Sm/Nd})^{\mathrm{PDAM}}$, $C_{\mathrm{Sm}}^{\mathrm{PDAM}}$, $(\mathrm{Sm/Nd})^{\mathrm{EER}}$, f_{EDR}, f_{PDAM}, $C_{\mathrm{Sm}}^{\mathrm{EDR}}$, $C_{\mathrm{Nd}}^{\mathrm{EDR}}$, $(^{147}\mathrm{Sm}/^{144}\mathrm{Nd})^{\mathrm{EDR}}$, $\varepsilon^{143}\mathrm{Nd}^{\mathrm{EDR}}$, $\varepsilon^{143}\mathrm{Nd}^{\mathrm{CC}}$, $\varepsilon^{142}\mathrm{Nd}^{\mathrm{EDR}}$, $\varepsilon^{142}\mathrm{Nd}^{\mathrm{BSE}}$, $C_{\mathrm{Nd}}^{\mathrm{BSE}}$, $C_{\mathrm{Sm}}^{\mathrm{BSE}}$, by using Eqs. (3)–(13), (15), and (17). So 12 out of the 14 constraints are incorporated at this point.
2. *Cost functions.* The success of any given model $\mathbf{m}$ is then judged by the following four normalized misfits:

$$F_1 = \frac{\varepsilon^{143}\mathrm{Nd}^{\mathrm{CC}} - E\left(\varepsilon^{143}\mathrm{Nd}^{\mathrm{CC}}\right)}{\sigma\left(\varepsilon^{143}\mathrm{Nd}^{\mathrm{CC}}\right)}, \tag{20}$$

$$F_2 = \frac{\varepsilon^{142}\mathrm{Nd}^{\mathrm{BSE}} - E\left(\varepsilon^{142}\mathrm{Nd}^{\mathrm{BSE}}\right)}{\sigma\left(\varepsilon^{142}\mathrm{Nd}^{\mathrm{BSE}}\right)}, \tag{21}$$

$$F_3 = \frac{\mathrm{EF} - E(\mathrm{EF})}{\sigma(\mathrm{EF})}, \tag{22}$$

$$F_4 = \frac{C_{\mathrm{Sm}}^{\mathrm{PDAM}} - E\left(C_{\mathrm{Sm}}^{\mathrm{PDAM}}\right)}{\sigma\left(C_{\mathrm{Sm}}^{\mathrm{PDAM}}\right)}, \tag{23}$$

and one penalty function:

$$F_5 = W_5\left[\Theta\left(C_{\mathrm{Nd}}^{\mathrm{EDR}} - C_{\mathrm{Nd}}^{\mathrm{EER}}\right) + \Theta\left(C_{\mathrm{Sm}}^{\mathrm{EDR}} - C_{\mathrm{Sm}}^{\mathrm{EER}}\right) + \Theta\left(\varepsilon^{143}\mathrm{Nd}^{\mathrm{EDR}} - \max\left(\varepsilon^{143}\mathrm{Nd}^{\mathrm{EDR}}\right)\right)\right], \tag{24}$$

where $E(x)$ and $\sigma(x)$ are the expectation and one standard deviation, respectively, of a variable x, W_5 is a weighting factor, and Θ is the step function: $\Theta(x) = 1$ for $x \geqslant 0$ and $\Theta(x) = 0$ for $x < 0$. EF denotes the enrichment factor for refractory lithophile elements and is calculated as $C_{\mathrm{Nd}}^{\mathrm{BSE}}/C_{\mathrm{Nd}}^{\mathrm{CI}}$ (or equivalently $C_{\mathrm{Sm}}^{\mathrm{BSE}}/C_{\mathrm{Sm}}^{\mathrm{CI}}$). The penalty function F_5 is to impose the inequality relations of (11), (18), and (19); $W_5 = 30$ is chosen to force them (mostly) satisfied during MCMC iterations. Solutions exceeding the *a priori* bounds of these parameters are excluded after iterations. Note that $\varepsilon^{143}\mathrm{Nd}^{\mathrm{CC}}$, $\varepsilon^{142}\mathrm{Nd}^{\mathrm{BSE}}$, and $C_{\mathrm{Sm}}^{\mathrm{PDAM}}$ are 'known' variables in this geochemical inverse problem but treated as a part of output parameters. This is one of tricks to make sampling efficient.

3. *The likelihood.* Finally, the likelihood is calculated as $L = \exp(-\chi^2/2)$, where

$$\chi^2 = \sum_{i=1}^{5} F_i^2. \tag{25}$$

Note that $C_{\mathrm{Sm}}^{\mathrm{PDAM}}$ is considered indirectly by the pair of $C_{\mathrm{Nd}}^{\mathrm{PDAM}}$ and $r_{\mathrm{Sm/Nd}}^{\mathrm{PDAM}}$. This is because considering directly $C_{\mathrm{Nd}}^{\mathrm{PDAM}}$ and $C_{\mathrm{Nd}}^{\mathrm{PDAM}}$ was found to make them 'sticky' parameters during MCMC iterations; i.e., Gibbs sampling was not able to efficiently sample these parameters during iterations and their auto-correlation exhibited much longer lags than others. The *a priori* bound for $r_{\mathrm{Sm/Nd}}^{\mathrm{PDAM}}$ is set to [1.0, 2.0] to cover that for $C_{\mathrm{Sm}}^{\mathrm{PDAM}}$ (Table 1). Similarly, the ratio $r_{\mathrm{Sm/Nd}}^{\mathrm{EER}}$ has the *a priori* range of (0, 1) so that the sampled parameter space of $C_{\mathrm{Nd}}^{\mathrm{EER}}$ and $C_{\mathrm{Sm}}^{\mathrm{EER}}$ is consistent with the expected range for $\varepsilon^{142}\mathrm{Nd}^{\mathrm{EER}}$. The enrichment factor criterion (Eq. (22)) is introduced to stabilize MCMC iterations by rejecting cosmochemically unrealistic solutions.

Though it uses mass-balance equations, the above method is different from usual mass-balance calculations. It is an inverse method to estimate simultaneously one of the end members of mass-balance calculations (the BSE composition) and the target of mass-balance calculations (the composition of a hidden reservoir).

3. RESULTS

Ten parallel Markov chains were used with randomly chosen initial guesses, and each chain was run for 4×10^7 iterations. These parallel runs resulted in virtually identical

a posteriori distributions, suggesting that convergence was achieved. Based on auto-correlation analysis, each chain was sampled at every few thousand iterations to collect statistically independent solutions, and solutions exceeding the *a priori* range of model parameters were then excluded. The total number of accepted solutions, all of which satisfy the given constraints exactly, is $\sim 1.6 \times 10^4$ from ten parallel runs. The *a posteriori* distributions of both known and unknown variables, which are summarized in Table 1 as well as Figs. 3–5 , are based on these MCMC solutions.

The maximum likelihood value for the mass fraction of EER, f_{EER}, is close to zero (Fig. 3). Because of the ^{142}Nd constraint (Eq. (15)), it cannot be zero, but as the distribution indicates, it is easier to find a solution when f_{EER} is smaller. Its first quartile, median, and third quartile are 0.03, 0.09, and 0.23, respectively (Table 1), meaning that the 25%,

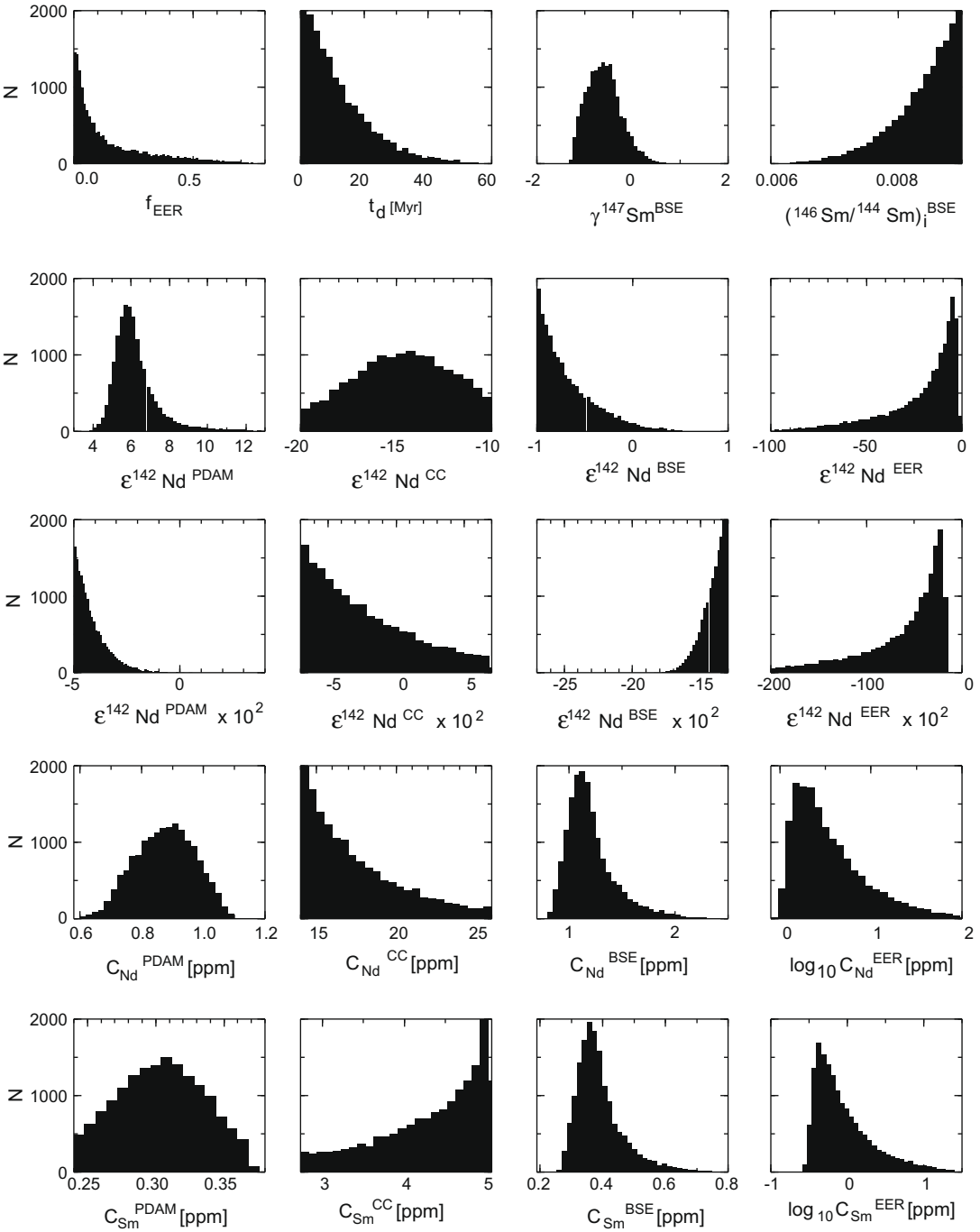

Fig. 3. The *a posteriori* distribution of model parameters based on $\sim 1.6 \times 10^4$ solutions obtained by Markov chain Monte Carlo simulations. The range of the abscissa is based on the *a priori* distribution for most parameters (see Table 1).

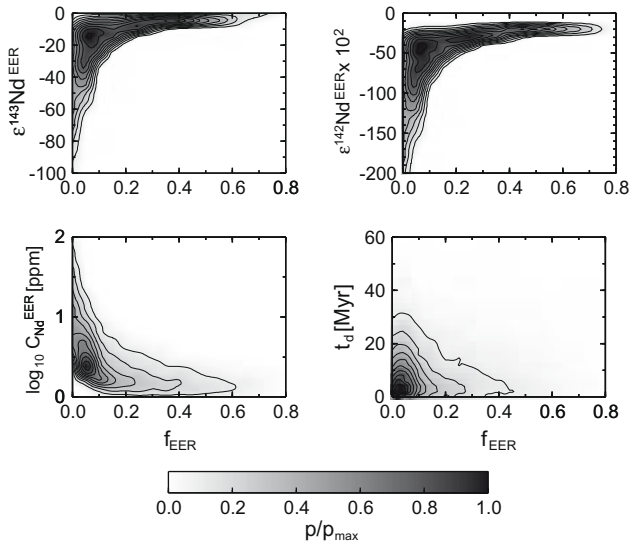

Fig. 4. The co-variations of some key variables ($\varepsilon^{143}Nd^{EER}$, $\varepsilon^{142}Nd^{EER}$, C_{Nd}^{EER}, and t_d) with the mass fraction of EER, f_{EER}, are shown as two-dimensional probability density distributions. Gray shading denotes normalized probability, and contours are drawn at every 0.1 interval.

50%, and 75% of solutions have f_{EER} smaller than these values. The distribution of the time of early differentiation, t_d, is similar but more of an exponential form, with the median of ~9 Myr. The largest possible t_d is ~50 Myr, and yet the Nd content of PDAM is lower than ~1 ppm for most solutions (Fig. 3). This is different from the calculation of Bourdon et al. (2008), which predicts unacceptably high Nd concentrations for PDAM when t_d is greater than 10 Myr. This is because we take into account parameter uncertainty; this study may be seen as a more generalized version of their calculation. Nevertheless, their main conclusion is still valid; 75% of our solutions have t_d less than ~17 Myr.

The chemical and isotopic compositions of EER are inversely correlated with its mass fraction (Fig. 4), because the product of these compositions with f_{EER} is what is constrained by mass balance. The log-medians of C_{Nd}^{EER} and C_{Sm}^{EER} are ~2.8 ppm and ~0.7 ppm, respectively, which are between the PDAM and CC values (Table 1). The median of $\varepsilon^{143}Nd^{EER}$ −14.4, similar to that of $\varepsilon^{143}Nd^{CC}$, whereas the median of $\varepsilon^{142}Nd^{EER}$ is very negative, being ~47 ppm lower than the terrestrial standard.

The comparison of the *a priori* and *a posteriori* distributions for variables related to PDAM, CC, and BSE is informative. For example, $(^{146}Sm/^{144}Sm)_i^{BSE}$ and C_{Sm}^{CC} prefer higher values within the given *a priori* ranges, whereas $\varepsilon^{143}Nd^{BSE}$ and C_{Nd}^{CC} show opposite trends. More important, it is difficult to have solutions with $\varepsilon^{142}Nd^{BSE}$ lower than −0.18 (Fig. 3). This may be understood from Eq. (10); in order to make $\varepsilon^{142}Nd^{BSE}$ more negative, we need to raise $(^{147}Sm/^{144}Nd)^{EDR}$, but this isotopic ratio is constrained by the present-day CC and PDAM compositions. In other words, it is impossible to find a self-consistent set of model parameters (differentiation age, reservoir size, elemental and isotopic compositions for CC, PDAM, BSE, EDR, and EER) if $\varepsilon^{142}Nd^{BSE}$ is too negative.

In Fig. 5a, the *a posteriori* distributions for the Nd and Sm concentrations of various geochemical reservoirs are compared. The mass-weighted average of the EER composition is found to be close to the line of the chondritic Sm/Nd ratio. Those which deviate significantly from the chondritic ratio do not contribute much to mass balance as they correspond to small f_{EER}. A compositional trend defined by mantle peridotites runs through PDAM and CC, and the average EER composition is also found on this upper mantle trend. We calculate the slope of early differentiation trend defined as:

$$\frac{\log C_{Sm}^{EER} - \log C_{Sm}^{EDR}}{\log C_{Nd}^{EER} - \log C_{Nd}^{EDR}} \tag{26}$$

for each solution, and its probability distribution is shown in Fig. 5b. The bulk of the solutions exhibits the early differentiation trend indistinguishable from the upper mantle trend. The significance of this finding will be discussed next.

4. DISCUSSION

4.1. Early differentiation at low pressures?

Fig. 5 suggests that the hypothetical early differentiation process may be similar to mantle melting in the upper mantle. This by itself does not preclude the possibility of high-pressure fractionation because there are not enough experimental constraints on element partitioning at lowermost mantle conditions. We may still argue, however, that the strong fractionation of Nd with respect to Sm, which is expected for the perovskite-melt system (Corgne et al., 2005), is not a favorable solution. It is easier to construct a self-consistent mass balance if the early differentiation took place along the upper mantle trend.

We may then have an interesting geodynamical problem; if EER was formed by melting in the upper mantle, how can it be sequestered for the rest of Earth's history? Early (basaltic) crust may become eclogite if crust is thick enough

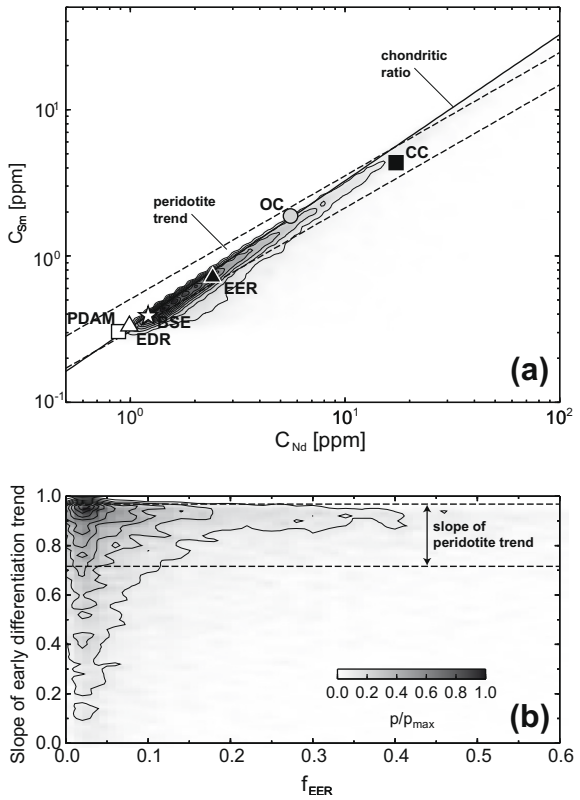

Fig. 5. (a) The relative locations of silicate reservoir compositions in the chemical space spanned by Nd and Sm. Symbols denote their mass-weighted averages, defined as $\sum_i f_x^i C_p^{x,i} / \sum_i f_x^i$, where f_x^i and $C_p^{x,i}$ represent the ith MCMC solutions for the mass fraction of a reservoir x and its content of element p, respectively. Gray shading represent the *a posteriori* distribution of the EER composition. As in Fig. 4, gray shading denotes normalized probability, and contours are drawn at every 0.1 interval. Also shown are the composition trend exhibited by upper-mantle rocks (dashed lines) (Lyubetskaya and Korenaga, 2007a), the chondritic Sm/Nd ratio (solid line) (Lodders and Fegley, 1998), and the composition of oceanic crust (OC, gray circle), which is obtained by multiplying Hofmann (1988)'s estimate on average MORB composition by 0.5, to take into account the effect of crustal fractionation. (b) The covariation of the early differentiation trend in the Nd–Sm space as defined by Eq. (26) and f_{EER}. Dashed lines denote the range comparable with the upper mantle trend.

(>60 km or so), and dense eclogitic lower crust may delaminate and sink down. Whether it can go down to the core–mantle boundary is not obvious, however, because of the density crossover expected at the base of the transition zone (e.g., Ringwood and Irifune, 1988). In the absence of plate tectonics at the beginning of Earth's history, the foundering of crustal materials is likely to take place as blob-like convective instability, so the density crossover is a serious impediment to downwelling. Moreover, even if delaminated crust can somehow reach the base of the mantle, whether it can stay there indefinitely is uncertain (e.g., Bourdon and Caro, 2007).

If EER is formed as protocrust, another way to hide (or lose) it is impact erosion (e.g., Halliday and Porcelli, 2001; O'Neill and Palme, 2008), which may be more likely than sequestering in the deep mantle, given frequent planetesimal collisions during the growth of the proto-Earth. Bourdon et al. (2008) argued against the formation of a deep EER by magma ocean differentiation on the basis of the required short time scale (i.e., $t_d < \sim 10$ Myr), and the present study provides an independent petrological argument, which seems to reinforce this chronological argument.

4.2. Depleted bulk silicate Earth and the weak chondrite assumption

If EER were lost into the space, EDR would correspond to the 'present-day BSE'. In this case, the constraint on $\varepsilon^{143}Nd^{EDR}$ (Eq. (11)) guarantees that the Sm/Nd ratio of the present-day BSE is within a few percent of the chondritic value, which may be called as the 'weak' chondrite assumption on the BSE composition (Korenaga, 2008). This assumption was adopted previously by Lyubetskaya and Korenaga (2007a), so their BSE composition should be comparable with the EDR composition derived in this study. In the limit of $f_{EER} \to 0$, C_{Nd}^{EDR} approaches 0.99 ± 0.09 ppm, which corresponds to the enrichment factor of 2.1 ± 0.20 (mean and one standard deviation) if the contribution of C_{Nd}^{EER} is ignored. This is surprisingly close to the estimate of Lyubetskaya and Korenaga (2007a), who derived the enrichment factor of 2.16 ± 0.37 from the statistical analysis of more than 10 different RLEs (Al, Ca, Sc, Ti, La, Ce, Nd, Sm, Eu, Tb, Yb, and Lu). This study uses only two RLEs (Nd and Sm), but it seems to be compensated well by the consideration of their isotopic information.

In the BSE model of Lyubetskaya and Korenaga (2007a), this enrichment factor was assumed for all other RLEs (including U and Th), and the BSE K content is then estimated using BSE K/U and K/La ratios. The corresponding BSE heat production is 16 ± 3 TW (Lyubetskaya and Korenaga, 2007b). Conversely, one may argue for varying enrichment factors among RLEs by adopting the impact erosion hypothesis (e.g., O'Neill and Palme, 2008). As protocrust (i.e., EER) would be more enriched in more incompatible elements, its loss by impact erosion is expected to result in the greater depletion of more incompatible elements in the present-day BSE (i.e., EDR). Even if the Sm/Nd ratio of EDR is only a few percent greater than the chondritic value, for example, Sm/U could be greater than chondritic by a few tens of percent. O'Neill and Palme (2008) suggested that the assumption of a constant enrichment factor may have resulted in overestimating heat-producing elements in previous BSE models and that the use of smaller enrichment factors for highly incompatible elements may resolve some of long-standing geochemical puzzles such as the missing Ar paradox and the helium and heat flux imbalance. This interesting possibility, however, can be questioned from at least two perspectives.

First, those 12 RLEs used by Lyubetskaya and Korenaga (2007a) span a range of geochemical compatibility (see their Fig. 4), and yet a BSE point can still be found along the upper mantle trend assuming the constant enrichment factor for all of these RLEs. In other words, the compositional trend of upper-mantle rocks does not seem to

support widely varying enrichment factors. Second, variable enrichment factors are not necessary to resolve the aforementioned geochemical paradoxes. These paradoxes, all of which are based on the claimed inability to close a self-consistent mass balance, can simply be explained by using a slightly lower (but still constant) enrichment factor (i.e., 2.16 ± 0.37, Lyubetskaya and Korenaga, 2007a) than adopted by previous BSE models (2.5–3.0, Hart and Zindler, 1986; McDonough and Sun, 1995; Palme and O'Neill, 2003) and by taking into account the uncertainty of the PDAM and CC composition models. Adding the PDAM model of Langmuir et al. (2005) and the CC model of Rudnick and Gao (2003), for example, approximately recovers the BSE model of Lyubetskaya and Korenaga (2007a), and such successful mass balance validates their constant enrichment factor. An important question is how the enrichment factor has been estimated in previous BSE models, and as discussed by Lyubetskaya and Korenaga (2007a) (see their Section 5.1), it is difficult to justify the high value of 2.8 ± 0.2 by Palme and O'Neill (2003), which originates in their unwarranted assumptions on the BSE Mg and Fe contents. Also, the helium and heat flux imbalance (O'Nions and Oxburgh, 1983) is actually expected from Earth's thermal budget (see Section 3.4 of Lyubetskaya and Korenaga (2007b) for full discussion) and does not constitute a paradox to begin with.

Whereas impact erosion may be a physically viable mechanism to remove EER from Earth, therefore, its consequence in terms of the present-day geochemical budget may not be adequately captured by a simple fractionation model. Secondary differentiation within protocrust and the loss of its upper fraction by impact, for example, might invalidate such simple model if the role of accessory minerals is taken into account (Watson and Harrison, 1984). An important observational constraint on the present-day BSE composition (and thus on the outcome of planetary accretion) may come from a better characterization of the PDAM composition. Estimating the PDAM composition is a challenging task because one has to deal with the compositional variability of MORB and OIB and arrive at a volumetric average of their source mantle compositions. As discussed by Korenaga (2008) (Section 2.1.2), existing PDAM (or DM) models do not meet this challenge in a satisfactory manner. Our inversion results for the Nd and Sm composition of PDAM (Table 1) are not depleted as that of Workman and Hart (2005) but not enriched as that of Langmuir et al. (2005) either. The median of $\varepsilon^{143}Nd^{PDAM}$ is ~6, which is at the low side of MORB values (close to the average of Indian MORB), so some contribution from OIB source mantle is evident. Future geoneutrino measurements may provide independent constraints on the U and Th contents of PDAM (e.g., Dye et al., 2006).

Regarding the depleted nature of the present-day BSE, it is important to recognize that its relatively low heat production with respect to surface heat loss (~46 TW (Jaupart et al., 2007)) does not pose a geodynamical problem (Korenaga, 2003, 2006). Secular cooling plays a significant role in Earth's thermal budget. The notion of thermal equilibrium (i.e., having internal production comparable to surface heat loss) has been persistent in the geochemical literature (e.g., Allegre, 2002; O'Neill and Palme, 2008), and this situation may be understandable given how our understanding of Earth's thermal budget has evolved in the last 100 years or so (see Section 5.2 of Korenaga (2008)).

5. CONCLUSION

This study was motivated by questions on the validity of existing BSE models, because recent debates on the origin of a hidden geochemical reservoir may undermine the common trend assumption adopted by those models. Constructing a self-consistent framework for global mass balance without using the common trend assumption requires us to estimate the compositions of BSE and a hidden reservoir simultaneously, and we were able to implement one possible approach following the early differentiation hypothesis. Because of the nontrivial uncertainty of available observational constraints, it is formulated as a nonlinear inverse problem, and we devised an efficient MCMC algorithm to explore the permissible model space extensively.

The early differentiation trend delineated by our inversion turned out to be indistinguishable from the upper mantle trend, thus justifying the common trend assumption. Also, our estimate for the timing of early differentiation reinforces the chronological argument against the formation of a hidden reservoir in the deep mantle (Bourdon et al., 2008). The loss of an early enriched reservoir by impact erosion appears to be a more realistic mechanism to explain the slightly nonchondritic nature of the present-day BSE; i.e., a hidden reservoir may have been lost into the space and does not have to reside within the Earth. This study thus happens to support the existing BSE model of Lyubetskaya and Korenaga (2007a), because it is the only model that is built on approximate (instead of strict) chondritic constraints and is consistent with the absence of a hidden reservoir within the mantle.

ACKNOWLEDGMENTS

This work was sponsored by the U.S. National Science Foundation under Grant EAR-0449517. This paper has benefited from constructive reviews by Bernard Bourdon and two anonymous reviewers and from thoughtful editorial handling by Fred Frey and Frank Podosek.

REFERENCES

Allegre C. J. (2002) The evolution of mantle mixing. *Phil. Trans. R. Soc. Lond. A* **360**, 2411–2431.

Allegre C. J., Hart S. R. and Minster J.-. F. (1983) Chemical structure and evolution of the mantle and continents determined by inversion of Nd and Sr isotopic data, II. Numerical experiments and discussion. *Earth Planet. Sci. Lett.* **66**, 191–213.

Allegre C. J., Hofmann A. and O'Nions K. (1996) The argon constraints on mantle structure. *Geophys. Res. Lett.* **23**, 3555–3557.

Anderson D. L., Tanimoto T. and Zhang Y. S. (1992) Plate tectonics and hotspots; the third dimension. *Science* **256**, 1645–1651.

Bennett V. C. (2003) Compositional evolution of the mantle. In *Treatise on Geochemistry*, vol. 2 (eds. H. D. Holland and K. K. Turekian). Elsevier, pp. 493–519.

Bourdon B. and Caro G. (2007) The early terrestrial crust. *C.R. Geosci.* **339**, 928–936.

Bourdon B., Touboul M., Caro G. and Kleine T. (2008) Early differentiation of the Earth and the Moon. *Phil. Trans. R. Soc. Lond. A* **366**, 4105–4128.

Boyet M. and Carlson R. W. (2005) ^{142}Nd evidence for early (>4.53 Ga) global differentiation of the silicate Earth. *Science* **309**, 576–581.

Boyet M. and Carlson R. W. (2006) A new geochemical model for the Earth's mantle inferred from ^{146}Sm–^{142}Nd systematics. *Earth Planet. Sci. Lett.* **250**, 254–268.

Burkhardt C., Kleine T., Bourdon B., Palme H., Zipfel J., Friedrich J. M. and Ebel D. S. (2008) Hf-W mineral isochron for Ca, Al-rich inclusions: age of the solar system and the timing of core formation in planetesimals. *Geochim. Cosmochim. Acta* **72**, 6177–6197.

Caro G., Bourdon B., Birck J.-L. and Moorbath S. (2003) ^{146}Sm–^{142}Nd evidence from Isua metamorphosed sediments for early differentiation of the Earth's mantle. *Nature* **423**, 428–432.

Caro G., Bourdon B., Birck J.-L. and Moorbath S. (2006) High-precision ^{142}Nd/^{144}Nd measurements in terrestrial rocks: constraints on the early differentiation of the Earth's mantle. *Geochim. Cosmochim. Acta* **70**, 164–191.

Caro G., Bourdon B., Halliday A. N. and Quitte G. (2008) Superchondritic Sm/Nd ratios in Mars, the Earth, and the Moon. *Nature* **452**, 336–339.

Christensen U. R. and Yuen D. A. (1984) The interaction of a subducting lithospheric slab with a chemical or phase boundary. *J. Geophys. Res.* **89**, 4389–4402.

Corgne A., Liebske C., Wood B. J., Rubie D. C. and Frost D. J. (2005) Silicate perovskite-melt partitioning of trace elements and geochemical signature of a deep perovskite reservoir. *Geochim. Cosmochim. Acta* **69**, 485–496.

DePaolo D. J. (1980) Crustal growth and mantle evolution: inferences from models of element transport and Nd and Sr isotopes. *Geochim. Cosmochim. Acta* **44**, 1185–1196.

Dye S. T., Gullian E., Learned J. G., Maricic J., Matsuno S., Pakvasa S., Varner G. and Wilcox M. (2006) Earth radioactivity measurements with a deep ocean anti-neutrino observatory. *Earth Moon Planets* **99**, 241–252.

Fei Y., Van Orman J., Li J., van Westrennen W., Sanloup C., Minarik W., Hirose K., Komabayashi T., Walter M. and Funakoshi K. (2004) Experimentally determined postspinel transformation boundary in Mg_2SiO_4 using MgO as an internal pressure standard and its geophysical implications. *J. Geophys. Res.* **109**, B02305. doi:10.1029/2003JB002652.

Frenkel D. and Smit B. (2002) *Understanding Molecular Simulation*, second ed. Academic Press, New York.

Fukao Y., Widiyantoro S. and Obayashi M. (2001) Stagnant slabs in the upper and lower mantle transition region. *Rev. Geophys.* **39**, 291–323.

Galer S. J. G., Goldstein S. L. (1996) Influence of accretion of lead in the Earth. In *Earth Processes: Reading the Isotopic Code*. Am. Geophys. Union Series. pp. 75–98.

Goldstein S. L., O'Nions R. K. and Hamilton P. J. (1984) A Sm–Nd isotopic study of atmospheric dusts and particulates from major river systems. *Earth Planet. Sci. Lett.* **70**, 221–236.

Halliday A. N. (2000) Terrestrial accretion rates and the origin of the Moon. *Earth Planet. Sci. Lett.* **176**, 17–30.

Halliday A. N. and Porcelli D. (2001) In search of lost planets: the paleocosmochemistry of the inner solar system. *Earth Planet. Sci. Lett.* **192**, 545–559.

Hart S. R. and Zindler A. (1986) In search of a bulk-earth composition. *Chem. Geol.* **57**, 247–267.

Hofmann A. W. (1988) Chemical differentiation of the Earth: the relationship between mantle, continental crust, and oceanic crust. *Earth Planet. Sci. Lett.* **90**, 297–314.

Hofmann A. W. (2003) Sampling mantle heterogeneity through oceanic basalts: isotopes and trace elements. In *Treatise on Geochemistry*, vol. 2 (eds. H. D. Holland and K. K. Turekian). Elsevier, pp. 61–101.

Hunt D. L. and Kellogg L. H. (2001) Quantifying mixing and age variations of heterogeneities in models of mantle convection: role of depth-dependent viscosity. *J. Geophys. Res.* **106**, 6747–6759.

Ito G. and Mahoney J. J. (2005) Flow and melting of a heterogeneous mantle: 2. Implications for a chemically nonlayered mantle. *Earth Planet. Sci. Lett.* **230**, 47–63.

Jacobsen S. B. and Wasserburg G. J. (1979) The mean age of mantle and crustal reservoirs. *J. Geophys. Res.* **84**, 7411–7427.

Jacobsen S. B. and Wasserburg G. J. (1980) Sm–Nd isotopic evolution of chondrites. *Earth Planet. Sci. Lett.* **50**, 139–155.

Jacobsen S. B. and Wasserburg G. J. (1984) Sm–Nd isotopic evolution of chondrites and achondrites, II. *Earth Planet. Sci. Lett.* **67**, 137–150.

Jaupart C., Labrosse S. and Mareschal J.-C. (2007) Temperatures, heat and energy in the mantle of the Earth. In *Treatise on Geophysics*, vol. 7 (ed. G. Schubert). Elsevier, Amsterdam, pp. 253–303.

Jochum K. P., Hofmann A. W., Ito E., Seufert H. M. and White W. M. (1983) K, U and Th in mid-ocean ridge basalt glasses and heat production, K/U and K/Rb in the mantle. *Nature* **306**, 431–436.

Katsura T., Yamada H., Shinmei T., Kubo A., Ono S., Kanzaki M., Yoneda A., Walter M. J., Ito E., Urakawa S., Funakoshi K. and Utsumi W. (2003) Post-spinel transition in Mg_2SiO_4 determined by high $P-T$ in situ X-ray defractometry. *Phys. Earth Planet. Int.* **136**, 11–24.

Kellogg L. H., Hager B. H. and van der Hilst R. D. (1999) Compositional stratification in the deep mantle. *Science* **283**, 1881–1884.

Korenaga J. (2003) Energetics of mantle convection and the fate of fossil heat. *Geophys. Res. Lett.* **30**(8), 1437. doi:10.1029/2003GL016982.

Korenaga J. (2004) Mantle mixing and continental breakup magmatism. *Earth Planet. Sci. Lett.* **218**, 463–473.

Korenaga J. (2005) Why did not the Ontong Java Plateau form subaerially? *Earth Planet. Sci. Lett.* **234**, 385–399.

Korenaga J. (2006) Archean geodynamics and the thermal evolution of Earth. In *Archean Geodynamics and Environments* (eds. K. Benn, J.-C. Mareschal and K. Condie). American Geophysical Union, Washington, DC, pp. 7–32.

Korenaga J. (2008) Urey ratio and the structure and evolution of Earth's mantle. *Rev. Geophys.* **46**, RG2007. doi:10.1029/2007RG000241.

Korenaga J. and Karato S. (2008) A new analysis of experimental data on olivine rheology. *J. Geophys. Res.* **113**, B02403. doi:10.1029/2007JB005100.

Labrosse S., Hernlund J. W. and Coltice N. (2007) A crystallizing dense magma ocean at the base of the Earth's mantle. *Nature* **450**, 866–869.

Langmuir C. H., Goldstein S. L., Donnelly K. and Su Y. J. (2005) Origins of enriched and depleted mantle reservoirs. *Eos Trans. AGU* **86**(52), Fall Meet. Suppl..

Lassiter J. C. (2004) Role of recycled oceanic crust in the potassium and argon budget of the earth: toward a resolution of the "missing argon" problem. *Geochem. Geophys. Geosyst.* **5**(11), Q11012. doi:10.1029/2004GC000711.

Liu J. S. (2001) *Monte Carlo Strategies in Scientific Computing*. Springer, New York.

Lodders K. and Fegley B. (1998) *The Planetary Science Companion*. Oxford University Press, New York.

Lugmair G. W. and Galer S. J. G. (1992) Age and isotopic relationships among the angrites Lewis Cliff 86010 and Angra dos Reis. *Geochim. Cosmochim. Acta* **56**, 1673–1694.

Lyubetskaya T. and Korenaga J. (2007a) Chemical composition of Earth's primitive mantle and its variance, 1, methods and results. *J. Geophys. Res.* **112**, B03211. doi:10.1029/2005JB004223.

Lyubetskaya T. and Korenaga J. (2007b) Chemical composition of Earth's primitive mantle and its variance, 2, implications for global geodynamics. *J. Geophys. Res.* **112**, B03212. doi:10.1029/2005JB004224.

Malaviarachchi S. P. K., Makishima A., Tanimoto M., Kuritani T. and Nakamura E. (2008) Highly unradiogenic lead isotope ratios from the Horoman peridotite in Japan. *Nat. Geosci.* **1**, 859–863.

McDonough W. F. and Sun S.-s. (1995) The composition of the Earth. *Chem. Geol.* **120**, 223–253.

Metropolis N., Rosenbluth A. W., Rosenbluth M. N., Teller A. H. and Teller E. (1953) Equations of state calculations by fast computing machines. *J. Chem. Phys.* **21**, 1087–1091.

Mosegaard K. and Tarantola A. (1995) Monte Carlo sampling of solutions to inverse problems. *J. Geophys. Res.* **100**, 12431–12447.

Naliboff J. B. and Kellogg L. H. (2007) Can large increases in viscosity and thermal conductivity preserve large-scale heterogeneity in the mantle? Phys. *Earth Planet. Int.* **161**, 86–102.

O'Neill H. S. C. and Palme H. (2008) Collisional erosion and the non-chondritic composition of the terrestrial planets. *Phil. Trans. R. Soc. Lond. A* **366**, 4205–4238.

O'Nions R. K. and Oxburgh E. R. (1983) Heat and helium in the Earth. *Nature* **306**, 429–431.

Palme H. and O'Neill H. S. C. (2003) Cosmochemical estimates of mantle composition. In *Treatise on Geochemistry*, vol. 2 (eds. H. D. Holland and K. K. Turekian). Elsevier, pp. 1–38.

Patchett P. J., Vervoort J. D., Söderlund U. and Salters V. J. M. (2004) Lu–Hf and Sm–Nd isotopic systematics in chondrites and their constraints on the Lu–Hf properties of the Earth. *Earth Planet. Sci. Lett.* **222**, 29–41.

Prinzhofer A., Papanastassiou D. A. and Wasserburg G. J. (1992) Samarium–neodymium evolution of meteorites. *Geochim. Cosmochim. Acta* **56**, 797–815.

Ranen M. C. and Jacobsen S. B. (2006) Barium isotopes in chondritic meteorites: implications for planetary reservoir models. *Science* **314**, 809–812.

Ringwood A. E. and Irifune T. (1988) Nature of the 650-km seismic discontinuity—implications for mantle dynamics and differentiation. *Nature* **331**, 131–136.

Robert C. P. and Cassela G. (2004) *Monte Carlo Statistical Methods*. Springer, New York.

Rudnick R. L. and Gao S. (2003) Composition of the continental crust. In *Treatise on Geochemistry*, vol. 3 (eds. H. D. Holland and K. K. Turekian). Elsevier, pp. 1–64.

Rudnick R. L. and Goldstein S. L. (1990) The Pb isotopic compositions of lower crustal xenoliths and the evolution of lower crustal Pb. *Earth Planet. Sci. Lett.* **98**, 192–207.

Salters V. J. M. and Stracke A. (2004) Composition of the depleted mantle. *Geochem. Geophys. Geosyst.* **5**, Q05004. doi:10.1029/2003GC000597.

Sambridge M. and Mosegaard K. (2002) Monte Carlo methods in geophysical inverse problems. *Rev. Geophys.* **40**, 1009. doi:10.1029/2000RG000089.

Schubert G., Turcotte D. L. and Olson P. (2001) *Mantle Convection in the Earth and Planets*. Cambridge, New York.

Stevenson D. J., Spohn T. and Schubert G. (1983) Magnetism and thermal evolution of the terrestrial planets. *Icarus* **54**, 466–489.

Turcotte D. L., Paul D. and White W. M. (2001) Thorium–uranium systematics require layered mantle convection. *J. Geophys. Res.* **106**, 4265–4276.

van der Hilst R. D., Widiyantoro S. and Engdahl E. R. (1997) Evidence for deep mantle circulation from global tomography. *Nature* **386**, 578–584.

van Keken P. E. and Ballentine C. J. (1998) Whole-mantle versus layered mantle convection and the role of a high-viscosity lower mantle in terrestrial volatile evolution. *Earth Planet. Sci. Lett.* **156**, 19–32.

von Neumann J. (1951) Various techniques used in connection with random digits. *Nat. Bur. Stand. Appl. Math. Ser.* **12**, 36–38.

Warren P. H. (2008) A depleted, not ideally chondritic bulk Earth: the explosive-volcanic basalt loss hypothesis. *Geochim. Cosmochim. Acta* **72**, 2217–2235.

Watson E. B. and Harrison T. M. (1984) Accessory minerals and the geochemical evolution of crustal magmatic systems: a summary and prospectus of experimental approaches. *Phys. Earth Planet. Int.* **35**, 19–30.

Workman R. K. and Hart S. R. (2005) Major and trace element composition of the depleted MORB mantle (DMM). *Earth Planet. Sci. Lett.* **231**, 53–72.

Zindler A. and Hart S. (1986) Chemical geodynamics. *Annu. Rev. Earth Planet. Sci.* **14**, 493–571.

Associate editor: Frederick A. Frey